EXPLORING NUCLEAR STRUCTURE IN ULTRAPERIPHERAL COLLISIONS*

Anna M. Staśto

Department of Physics, Penn State University, University Park, PA 16802, USA

Received 11 December 2025, accepted 18 December 2025, published online 8 April 2026

In this article, ultraperipheral collisions of nuclei are discussed with focus on the probes of nuclear structure. Calculations for the open charm production in UPC collisions of PbPb at the LHC are described and compared with the experimental data from the CMS experiment.

DOI:10.5506/APhysPolB.57.4-A5

1. Introduction

Relativistic heavy-ion collisions have been studied extensively at Relativistic Heavy Ion Collider (RHIC) and Large Hadron Collider (LHC). The primary goal of these experiments is the creation of the quark–gluon plasma, which is expected to have been present at the very early stages of the universe. Various measurements explore the properties of the formed quark–gluon plasma. These experiments aim to answer the fundamental question about the behavior of strong interactions in the regime of high energy and density, including mapping of the phase diagram of Quantum Chromodynamics (QCD). In addition, they can provide information about the nuclear structure, and the role of initial and final states in a variety of processes. The standard heavy-ion collisions have large multiplicities of produced particles, which depend on energy and centrality of events. These events are typically characterized by the impact parameters which are less than the sum of radii of two incoming nuclei.

On the other hand, in a typical bunch crossing in an accelerator, nuclei pairs can interact when the impact parameter exceeds the sum of the two radii. In such a scenario, the electromagnetic interaction dominates and the hadronic one is strongly suppressed. These type of events are called ultraperipheral collisions (UPC), for reviews, see [1, 2]. At high energies, the strong electromagnetic fields surrounding the ultrarelativistic ions can

* Based on a lecture given at the 65$^{\text{th}}$ Jubilee Cracow School of Theoretical Physics, Zakopane, Tatra Mountains, Poland, 14–21 June, 2025.

be viewed as a flux of quasi-real photons. This flux is calculable thanks to the use of the equivalent photon approximation (EPA) method [3–6]. It can be viewed as interaction of nuclei with strong electromagnetic fields, and thus, in the heavy-ion colliders, one can realize photon–nuclei and photon–photon collisions. In the ultraperipheral collisions one can study photon–photon interactions, which can serve as tests of Quantum Electrodynamics, and the Standard Model in general, but also can provide opportunities to test beyond Standard Model physics. The photo-nuclear reactions, can in turn offer possibilities to explore the nuclear structure, both through exclusive and inclusive processes.

In this article, I shall discuss ultraperipheral collisions, with special focus on the process of open heavy flavor production in ultraperipheral collisions as a test of nuclear structure. More details of the calculation for this process can be found in [7].

2. Photon flux from electrons and nuclei

The flux of photons in the ultraperipheral collisions of nuclei can be evaluated using the (EPA) developed by Fermi [3, 4], and then Weizsäecker [5] and Williams [6]. The core idea is to treat the electromagnetic field of a fast moving charged particle as the flux of equivalent quasi-real photons. The UPC cross section can then be obtained by a simple convolution of the flux of the quasi-real photons from the nucleus and the cross section of the interaction of the quasi-real photon with another nucleus (photo-nuclear reaction) or another photon (in photon–photon interactions).

A widely used parametrization for the photon flux from the nucleus in UPC is obtained in a pointlike approximation, where the details of the spatial extent of the nucleus are neglected, and the nucleus is treated as a pointlike charge. One advantage of this parametrization is that it has a closed analytic expression, see, for example, in [1]

$$f_{\gamma/A}(z) = \frac{2Z^2\alpha_{\rm em}}{\pi z}\left[\eta K_0(\eta)K_1(\eta) - \frac{\eta^2}{2}\left(K_1(\eta)^2 - K_0(\eta)^2\right)\right], \qquad (1)$$

with the dimensionless variable η defined as

$$\eta = \frac{z\, m_p\, b_{\rm min}}{\hbar c}\,. \qquad (2)$$

In Eq. (1), the function $f_{\gamma/A}(z)$ is the photon flux of the nucleus, where the argument z is the fraction of the energy of nucleus carried by the photon. Other constants appearing in this expression are: m_p, the proton mass, Z, atomic number ($Z = 82$ for lead), $b_{\rm min}$, distance between the nuclei. Functions K_0, K_1 are modified Bessel functions. Following [8–10], we take

the impact parameter between nuclei to be $b_{\min} = 2R = 14.2$ fm, with $R = 7.1$ fm being the nuclear hard-sphere radius, to account for the finite size of the colliding nuclei. It is important to note that pointlike approximation is expected to work well for small z, but for large photon energies, more refined approaches should be used, which take into account the detailed geometry of the nucleus and charge distribution, see, for example, [10] for a recent detailed study on that topic.

The parametrization for the photon flux from nuclei, as given in Eq. (1) and scaled by z, is denoted by a red dotted line in Fig. 1. We see that the flux, rescaled by z, is fairly flat for low values of z, which is a reflection of the logarithmic behavior

$$z f_{\gamma/A}(z) \simeq \frac{2Z^2\alpha_{\rm em}}{\pi} \log\left(\frac{1}{\eta}\right)$$

as $z \to 0$. On the other hand, at intermediate z, it exhibits a sharp cutoff due to the presence of the Bessel functions K_0 and K_1, which fall off exponentially with η. As a result, the photon flux from nuclei becomes negligible for $z > 0.1$.

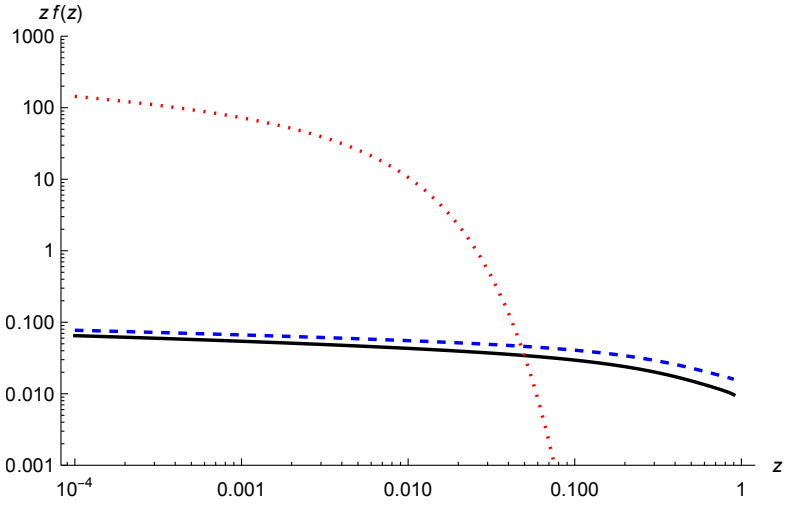

Fig. 1. Photon flux scaled by z as a function of the fractional photon energy z. The electron flux of Eq. (3) is shown for $Q^2_{\rm max} = 0.01$ GeV^2 (solid black) and $Q^2_{\rm max} = 2$ GeV^2 (dashed blue), while the lead–nucleus flux of Eq. (1) appears as a red dotted line. Figure from [7].

For comparison, we also show in Fig. 1 the photon flux from electrons, indicated by the solid black and dashed lines. The photon flux from electrons (see, for example, [11]) is given by

$$f_{\gamma/e}(z) = \frac{\alpha_{\rm em}}{2\pi}\left[\frac{1+(1-z)^2}{z}\log\left(\frac{Q^2_{\rm max}(1-z)}{(m_e z)^2}\right) + 2m_e^2 z\left(\frac{1}{Q^2_{\rm max}} - \frac{1-z}{(zm_e)^2}\right)\right], \quad (3)$$

where z is the fraction of the energy of the electron carried by the photon, m_e is the electron mass, $Q^2_{\rm max}$ is the limit on the (negative) photon virtuality, and $\alpha_{\rm em}$ is the electromagnetic coupling. In Fig. 1, the solid black curve corresponds to $Q^2_{\rm max} = 0.01$ GeV^2, and the dashed blue line uses $Q^2_{\rm max} = 2$ GeV^2. These two choices correspond to the two distinct experimental scenarios at the HERA collider. The electron flux is very flat over the entire range of z, and has a non-negligible dependence on $Q^2_{\rm max}$. In the limit of low z, the electron flux also contains a logarithm,

$$f_{\gamma/e}(z) \simeq \frac{\alpha_{\rm em}}{\pi}\left[\frac{1}{z}\log\left(\frac{Q^2_{\rm max}}{(m_e z)^2}\right)\right].$$

For large photon energy fractions, the photon flux from the electron is much flatter than in the nucleus case and extends to large values of the photon energy.

3. UPC physics

As mentioned in the introduction, UPCs offer ample opportunities for testing a variety of phenomena in photon–photon and photo-nuclear reactions. For example, photon–photon processes can be used to test the Quantum Electrodynamics and the Standard Model in general, as well as possible signatures of beyond Standard Model physics. A notable example is the possibility of the precision measurement of the anomalous magnetic moment of the τ lepton. The anomalous magnetic moment is defined as $a_l = (g_l - 2)/2$, where $l = e, \mu, \tau$ and g_l is the gyromagnetic ratio which relates the magnetic dipole moment of the charged lepton l to its spin, and is equal to 1 in classical physics and 2 in the Dirac equation. Quantum corrections introduce deviations of the gyromagnetic ratio from 2. This quantity has been the subject of intense experimental and theoretical efforts since a long time. Due to the very short τ lifetime, standard spin precession methods to measure a_τ are not applicable. However, the scattering processes of $\gamma\gamma \to \tau^-\tau^+$, accessible at high-energy accelerators, can probe the $\gamma\tau\tau$ vertex. Until recently the best experimental limits were set by the DELPHI experiment in e^+e^- collisions at LEP [12]. The LHC opened up new possibilities in this area, and several measurements by ATLAS [13] and CMS [14, 15] were performed both in pp and PbPb collisions, with great precision in a wide kinematic range of masses. For more information and other possibilities of the $\gamma\gamma$ physics, see the excellent review [16].

3.1. Exclusive vector meson photoproduction

Exclusive processes of vector mesons have been studied extensively in electron–proton collisions at the HERA collider, see, for example, [17–20]. In this process, the electron and proton interact to give in the final state a scattered electron, proton as well as a vector meson, for example $\rho, \phi, J/\psi$ or Υ. At HERA, this process has been measured both in electroproduction (when the negative virtuality of the photon is larger than zero) and also in photoproduction (when the exchanged photon is quasi-real). Since the process is exclusive with the elastically scattered proton, the requirement of the rapidity gap between the vector meson and the scattered proton implies the necessity for the color singlet exchange, which at the lowest order can be modeled via two gluons. The lowest order formula, which describes the cross section at zero momentum transfer $t = 0$, for this process, is given by [21] (see also [22])

$$\left.\frac{\mathrm{d}\sigma^{\gamma^* p \to Vp}}{\mathrm{d}t}\right|_{t=0} = \frac{\Gamma_{ee} M_V^3 \pi^3}{48\alpha_{\mathrm{em}}} \left[\frac{\alpha_{\mathrm{s}}\left(\bar{Q}^2\right)}{\bar{Q}^4} x g\left(x, \bar{Q}^2\right)\right]^2 \left(1 + \frac{Q^2}{M_V^2}\right), \tag{4}$$

where Γ_{ee} is the electronic width for the vector meson, $\bar{Q}^2 = (Q^2 + M_V^2)/4$, $x = (Q^2 + M_V^2)/(W^2 + M_V^2)$ and M_V is the mass of the vector meson, and W is the γp center-of-mass energy. The above formula can be applied in the photoproduction as well, but it is applicable provided the vector meson is heavy, like J/ψ or Υ. The distinct feature of this process is the fact that it is sensitive to the square of the gluon density $xg(x, \bar{Q}^2)$, thus providing access to the small-x region, when the center-of-mass energy W is sufficiently high.

The H1 and ZEUS experiments at the HERA collider performed many measurements of the elastic diffractive photoproduction for various vector mesons. It has been found that the cross section rises with the energy W, with behaviour that can be approximately parametrized as

$$\sigma \sim W^{\delta}, \tag{5}$$

where the δ exponent rises when the masses of the vector mesons are increasing, signalling the transition from the soft to the hard regime, see, for example, [23].

The elastic diffractive photoproduction of vector mesons can also be measured in UPCs, by requiring both initial particles (proton or nucleus) to stay intact after scattering and requiring large rapidity gaps in the final state. In PbPb collisions, one lead nucleus is a source of the photon flux, which then interacts in a photoproduction process with another nucleus to produce a vector meson diffractively. In pPb collisions, again the photon comes from lead nucleus, but the target is the proton, allowing for extending the range of

energy previously probed at HERA. The measurements, particularly those of charmonium, were performed at the LHC in a wide energy range, see, for example, [24–28]. They offer a long lever arm in energy, ideal for testing the gluon density and its evolution at moderate scales. The UPC pPb collisions provide an opportunity to probe the gluon in the proton, whereas PbPb collisions test the nuclear gluon density. There has been extensive theoretical effort to describe these measurements, see, for example, [29–35]. The measurement in pPb can be used to test various scenarios of the gluon evolution at small x, and allow for the search of saturation effects in the proton target. The measurements of the exclusive production of J/ψ mesons in coherent photon–Pb scatterings [25–28, 36] allow for testing the nuclear density in the nucleus where the nuclear modification effects are expected to be rather large. Indeed, the measurements have provided strong experimental indications of a significant suppression of the PDF for gluons in lead nucleus at very small values of x.

These exclusive measurements provide an unprecedented coverage to low values of x, however they are somewhat limited by the fact that the gluon density is only probed at mass scales corresponding to the vector meson mass. Another problem is the necessity to model the wave function of the vector meson, which can be the source of significant theoretical uncertainty.

3.2. Open charm production

An inclusive open charm production in photon–nucleus collision offers a unique window into probing the gluon density in the nucleus. The process is illustrated in the left panel of Fig. 2, where the incoming nucleus undergoes an ultraperipheral collision, and as a result, the incoming photon interacts with the parton (most likely a gluon) from the other nucleus to produce a heavy quark pair.

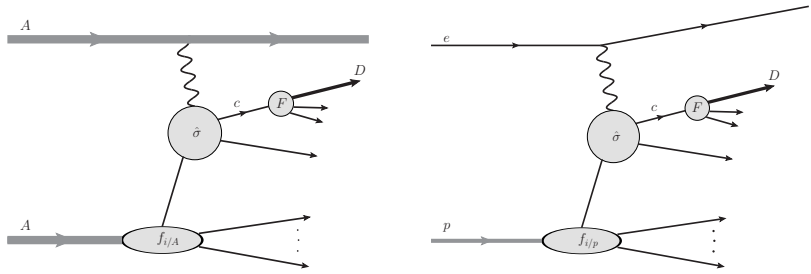

Fig. 2. Schematic description of the inclusive D meson production in ultraperipheral heavy-ion collisions (left) and in electron–proton collisions (right). Here, $f_{i/p}$ and $f_{i/A}$ denote PDF in the proton or nucleus, F fragmentation function, and $\hat{\sigma}$ hard scattering process.

The heavy-quark (in this case, charm) fragments into a meson (for example, D^0), which is then observed in the experiment. The advantage of this process is the possibility of scanning wide range of scales given by the transverse mass: $m_{\mathrm{T}} = \sqrt{p_{\mathrm{T}}^2 + m_c^2}$. Since it is an inclusive process, one can test the factorization theorem and the universality of the parton distribution functions. Since the charm quark is predominantly produced in the photon–gluon fusion, this process gives access primarily to the gluon density, and in the PbPb collisions, it is sensitive to the nuclear gluon density. Thus, this process allows us to measure the nuclear modification of the gluon PDF and test parton evolution, including the nonlinear effects. This process is very similar to the one in electron–proton collisions, see the right panel of Fig. 2, which has been measured in the experiments at the HERA collider [37–39].

The differential cross section for the inclusive D meson production can be measured as a function of transverse momentum and rapidity. The kinematic dependence on these variables can then be used to estimate the sensitivity of this process to the (x, Q^2) range of the gluon density in the process. The scale in the gluon density can be taken as the transverse mass $m_{\mathrm{T}}^2 = p_{\mathrm{T}}^2 + m_c^2$, and the longitudinal momentum carried by the parton can be approximated as $x \simeq m_{\mathrm{T}}/\sqrt{s_{NN}}\, \mathrm{e}^{-y_c}$. This range, for the case of the CMS kinematics at $\sqrt{s_{NN}} = 5.36$ TeV, is schematically depicted in Fig. 3.

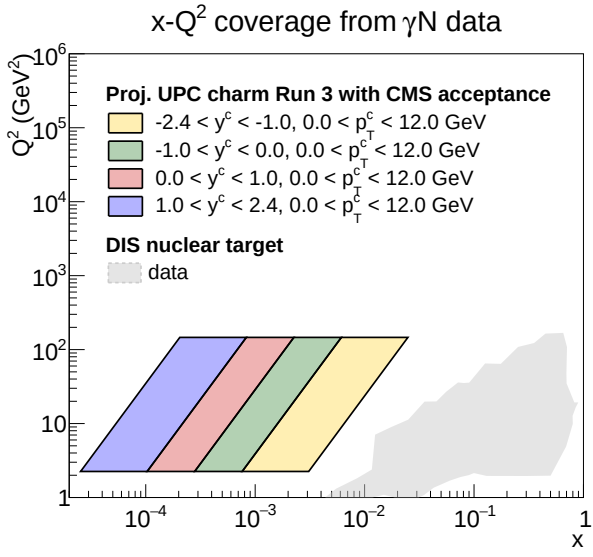

Fig. 3. x and Q^2 coverage charm production in UPCs collisions. Grey area indicates the existing coverage from fixed-target deep-inelastic photonuclear measurements [40]. Figure from [7].

We observe that for the p_T and rapidity range accessible in the CMS kinematics, the values of x, which can be achieved, are below 10^{-4} for scales that can be lower than 10 GeV^2 provided that the measurements extends to very low transverse momenta. Of course, this is rather a crude estimate, given that the kinematics of the second quark is effectively integrated over, and fragmentation effects are not taken into account. Nevertheless, it gives a good first-order estimate of the possible kinematical region, in which the nuclear gluon density can be probed in this process.

3.2.1. Heavy-quark photoproduction cross section

The heavy quark photoproduction cross section can be calculated using collinear factorization, since the transverse mass m_T provides a hard scale, and thus makes a perturbative calculation possible. In Ref. [7], the differential cross section for heavy-quark production was calculated using the FONLL framework [41, 42]. It was updated and benchmarked against the HERA data, and subsequently adapted to the UPC case. The FONLL approach connects the low transverse momentum region, where the fixed-order approach can be used, to the high transverse momentum region, where large logarithms $\ln p_T/m_c$ are resummed. The matching of the FONLL resummed cross section can be expressed as [42, 43]

$$\text{FONLL} = \text{FO} + (\text{RS} - \text{FOM0}) \times G(m, p_T) \ , \tag{6}$$

where FO denotes fixed order, which is an exact calculation at NLO accuracy for massive heavy quarks [44, 45]. RS denotes the resummed result and FOM0 is the massless limit of a fixed-order FO without terms suppressed by powers of mass m, while logarithms of the mass are retained. Finally, the resummed formula must be supplemented by the damping function, denoted by $G(m, p_T)$. This function is rather arbitrary, but it must be regular in p_T, and must approach unity at large transverse momenta.

The cross section contains both pointlike and resolved contributions. That is, a pointlike contribution contains the partonic cross section for the photon–parton interaction convoluted with the parton distribution function in the incoming hadron (proton or nucleus). The resolved contribution is obtained by convoluting the parton–parton elementary cross section together with the PDF from the photon and the proton (or a nucleus). It is worth noting that the distinction between these two contributions is arbitrary, as they are not observable quantities by themselves, only the sum can be measured in the complete cross section. Strictly speaking, they are related beyond the leading order, see discussion in [42].

The differential cross section for the heavy-quark production needs as an input the parton distribution function in the target nucleon or nucleus, as well as the parton distribution in the photon, for the resolved contribution as discussed above. For the nuclear PDF, two parametrizations have been used for the lead nucleus, the EPPS21 [46] and nNNPDF3.0 [47]. Both parametrizations have been fitted to the DIS fixed target data, as well as the data from the LHC pPb collisions. In particular, they include the LHCb data on the D^0 production. Both nuclear PDFs exhibit marked suppression of the gluon distribution at very low values of x. This is illustrated as an example in Fig. 4, where the nuclear ratio is shown for EPPS21 for the gluon density at scale $Q = 3.5$ GeV which roughly corresponds to the range probed in the CMS kinematics.

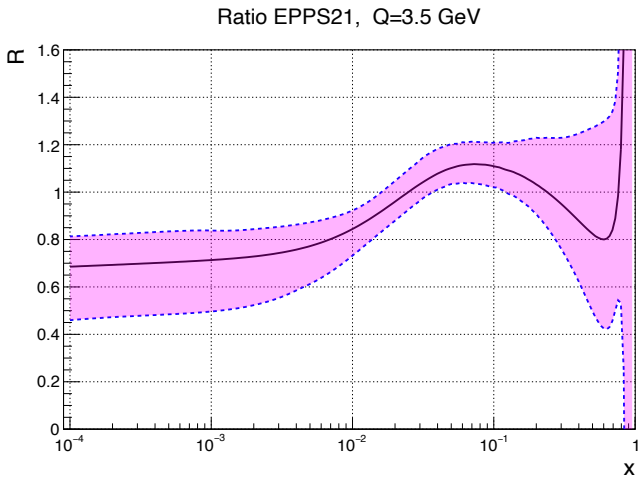

Fig. 4. Example of nuclear ratio for the gluon density from EPPS21 parametrization [46] as a function of x for scale $Q = 3.5$ GeV, with band corresponding to the PDF uncertainty.

In addition, for comparison, we have also used the proton PDF, CT18ANLO [48]. This was done in order to compare with the calculation, which does not include any nuclear effects (see Section 4).

For the resolved contribution, the photon PDF is needed, for which two parametrizations have been used: AFG [49] and GRV [50], and it was found that they give very similar results.

Finally, in order to describe the production of the D^0 meson, fragmentation function must be used, which parametrizes the fragmentation of a heavy quark into a heavy meson. This is a non-perturbative function, which needs to be parametrized, with parameters adjusted to fit the experimental data. It describes the distribution in the momenta of the mesons which emerge from

the fragmentation of the quarks. In analysis [7], we used two parametrizations: the Peterson–Schlatter–Schmitt–Zerwas (PSSZ) [51] and Braaten–Cheung–Fleming–Yuan (BCFY) [52] fragmentation functions.

3.2.2. Electromagnetic dissociation

For the case of charm production in electron–proton (or nucleus) collisions, the above ingredients described in the previous section are completely sufficient. The cross section for photon–proton (nucleus) can then be convoluted with the photon flux from the electron and calculations can be compared with the HERA data. This was originally done in [43] for the FONLL, for the H1 and ZEUS data on D^* production, and then recently in [7]. In the latest calculation, the FONLL was benchmarked against the HERA data with the latest parton distribution functions in the proton. However, in the UPC, the situation is more complicated. The UPC events are experimentally selected [53] by the 0nXn requirement. It means that there are no neutrons in one Zero Degree Calorimeter (ZDC), and this side likely corresponds to the nucleus emitting a photon. The other requirement is Xn, which means that there is at least one nucleon in the Zero Degree Calorimeter on the other side. This means that this was the nucleus emitting a parton. This requirement is augmented by the additional rapidity gap in the 0n direction in order to further suppress the hadronic activity. Such a condition is required in order to select photo-nuclear events and suppress the hadronic events, which are mainly coming from XnXn events, and the photon–photon processes mainly coming from 0n0n events.

However, such a requirement means that the process is not entirely inclusive. This has to be contrasted with the theoretical calculation which by definition is inclusive. What can, however, happen is that additional soft electromagnetic interactions can lead to the breakup of the nucleus, which, even if it is emitting a photon, can be subsequently broken up. Therefore, one has to include the possibility that a photonuclear event, in which the nucleus is broken by the electromagnetic interaction, is rejected by the 0nXn requirement. Hence, such a no-brekup probability has to be included in theoretical calculations. The crucial assumption is that this probability is dominated by soft processes, which can be treated as factorizable from the rest of the interaction. We included the no-breakup probability in the form of the effective photon flux, which has this effect folded in, see [10].

The size of the electromagnetic dissociation effect is illustrated in Fig. 5. The left plot shows the effective photon flux divided by the original flux. The reduction indicates the no-breakup probability. We observe that this reduction is largest for large photon energies, where it can reach down to 0.2 for

the largest photon energies. This is due to the fact that the probability of the electromagnetic dissociation is enhanced for small impact parameters, which also correspond to the region of the largest energies of the photons.

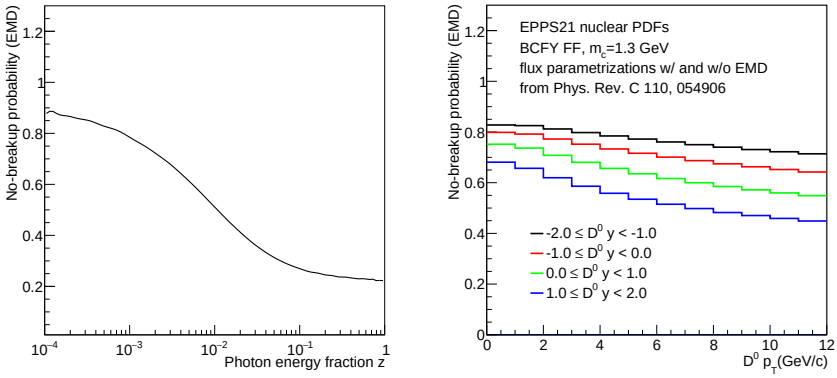

Fig. 5. Left: No-breakup probability (EMD) as a function of the photon energy fraction z. Right: No-breakup probability (EMD) as a function of the transverse momentum of the D^0 meson, in different intervals of the D^0 rapidity y. The photon fluxes used to compute these ratios are taken from [10]. Figure from [7].

The right plot in Fig. 5 shows the effect of this reduction when folded into the differential cross section for the D meson production. We present in this figure the ratio of the double differential cross section for D meson production as a function of transverse momentum in bins of rapidity, to the differential cross section obtained with the modified photon flux, which includes the no-breakup probability. We see that in general this ratio ranges from 0.83 to 0.68 for mesons in the lowest p_{T} bins in the range of 0 to 1 GeV, and from 0.71 to 0.45 for the transverse momenta from 11 to 12 GeV.

4. Description of the data on D^0 production in UPC at the LHC

In this section, we present a comparison of the theoretical calculations based on the GγA-FONLL framework with the data from CMS on the D^0 production in ultraperipheral collisions. These data [53] were obtained in PbPb collisions at $\sqrt{s_{NN}} = 5.36$ TeV, in the range of transverse momentum $2 < p_{\mathrm{T}} < 12$ GeV and rapidity between -2 to 2.

We start by showing in Fig. 6 a double differential cross section for the D^0 photoproduction in UPC in the CMS binning: three bins in p_{T} (2–5), (5–8), (8–12) GeV. For the lowest bin in p_{T}, there is only a single bin in rapidity $(-1, 1)$, while the two higher bins in p_{T} have 4 bins in rapidity, with the range $(-2, 2)$.

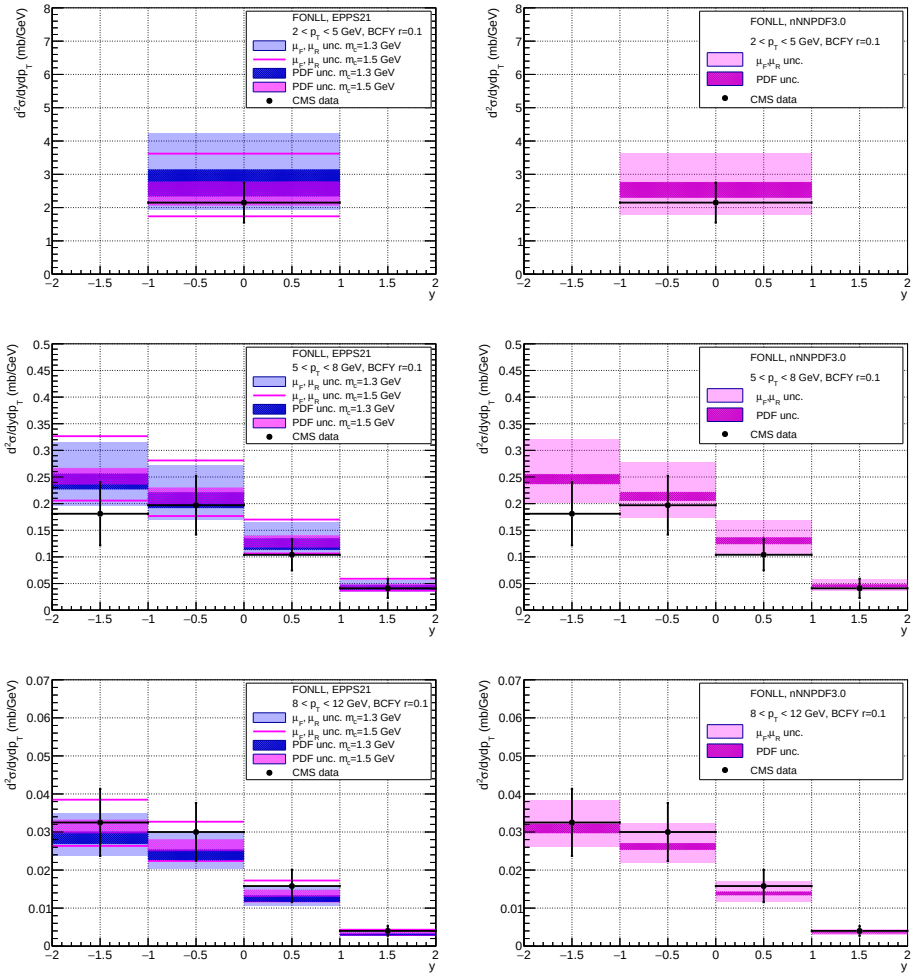

Fig. 6. Left column: rapidity distribution for the D^0 photoproduction in UPC PbPb collisions at the LHC at $\sqrt{s_{NN}} = 5.36$ TeV. Theoretical calculation is using EPPS21 [46] nuclear PDF. Top to bottom: three bins in p_{T}: (2–5), (5–8), (8–12) GeV. Light blue band: factorization and renormalization scale variation for $m_c = 1.3$ GeV, magenta lines band: factorization and renormalization scale variation and $m_c = 1.5$ GeV, dark blue band: EPPS21 [46] PDF uncertainty, $m_c = 1.3$ GeV. Magenta band: EPPS21 [46] PDF uncertainty, $m_c = 1.5$ GeV. The BCFY fragmentation function [52, 54] with parameter $r = 0.1$, and GRV [50] parametrization for the photon PDF. Data are from CMS [53]. Right column: the FONLL calculation is performed with nNNPDF3.0 nuclear parton distribution, charm mass set to $m_c = 1.5$ GeV.

In the left column, we show the calculations using the EPPS21 nuclear PDFs [46], while the right column in Fig. 6 is obtained using nNNPDF3.0 [47] nuclear PDF. For both cases, the BCFY [52] fragmentation function was used with parameter $r = 0.1$. The thinner (darker) bands indicate the PDF uncertainties, while the wider (lighter) bands correspond to the factorization (μ_F) and renormalization (μ_R) scale dependence in a seven-point variation scheme. That is, the variation is $1/2\mu_0 \leq \mu_R, \mu_F \leq 2\mu_0$ with $1/2 \leq \mu_R/\mu_F \leq 2$, and scale $\mu_0 = \sqrt{p_T^2 + m_c^2}$. For the EPPS21 calculation in the left column, two choices of charm masses were selected $m_c = 1.3$ GeV (blue) and $m_c = 1.5$ GeV (magenta), while for the nNNPDF3.0 calculation only with $m_c = 1.5$ GeV is shown.

The black points are the CMS data [53]. Overall, we observe a very good agreement between the data and theoretical calculations. The theoretical calculations seem to underestimate the data a bit at the highest p_T bin, an effect which was also observed in the comparison of the FONLL calculation with the HERA data, see [7]. However, it is still within the relatively large theoretical and experimental uncertainties, and it can also be affected by the choice and tuning of the fragmentation function. We observe in the left and right columns of Fig. 6 that the calculation with the higher charm mass $m_c = 1.5$ GeV tends to describe the data better. As observed and discussed in [43] and confirmed recently in [7], the higher charm mass results in a lower cross section at low values of p_T, but leads to a slightly higher cross section at high values of p_T. The latter effect is due to the reduced effect of the resummation of logarithms of $\ln p_T/m_c$.

Finally, in Fig. 7, we show the same CMS data [53] compared to the FONLL calculation using the CT18ANLO parton distribution function. This PDF is the proton baseline for the EPPS21 parametrization, see [46]. Therefore, the aim of this comparison is to test the agreement between the data and calculation in the absence of nuclear effects in theoretical predictions. We see from Fig. 7 that while in the two higher p_T bins, theoretical calculations are still reasonably consistent with the data, the lowest p_T bin shows a significant discrepancy. We clearly observe that the theoretical calculation with proton PDF overestimates the data in this bin, and is certainly higher than the calculations using the EPPS21 or nNNPDF3.0 nuclear PDFs in Fig. 6. This is the region where we expect suppression due to the nuclear shadowing, corresponding roughly to the same kinematic region selected when plotting the nuclear ratio in Fig. 4. Therefore, the CMS data clearly exhibit the need for including the nuclear effects (in this case, suppression) for the low-p_T values.

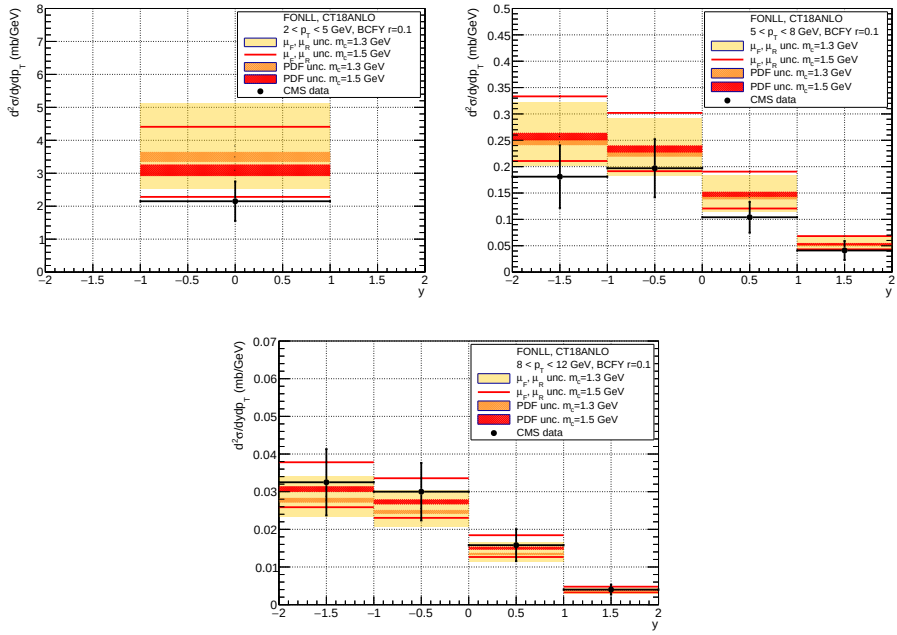

Fig. 7. Rapidity distribution for the D^0 photoproduction in UPC PbPb collisions at $\sqrt{s_{NN}} = 5.36$ TeV with the CT18ANLO proton PDF in p_{T} bins (2–5), (5–8), (8–12) GeV. Yellow band: FONLL calculation with factorization and renormalization scale variation for $m_c = 1.3$ GeV, red lines band: FONLL calculation with factorization and renormalization scale variation and $m_c = 1.5$ GeV, orange band: FONLL CT18ANLO PDF uncertainty, $m_c = 1.3$ GeV. Red band: FONLL CT18ANLO [46] PDF uncertainty, $m_c = 1.5$ GeV. The BCFY fragmentation function [52, 54] with parameter $r = 0.1$. Data are from CMS [53].

5. Conclusions

Ultraperipheral collisions of nuclei provide many opportunities for testing and exploring a variety of phenomena in particle and nuclear physics. Photon–photon collisions offer precision tests of the Standard Model and beyond, while photo-nuclear reactions allow for precise studies of nuclear structure. In this article, we described theoretical calculations for the process of inclusive charm production in UPC at the LHC. We extended the framework based on the FONLL resummation for heavy-quark production, previously developed for the electron–proton scattering, to ultraperipheral collisions by including the photon flux from the nucleus and the survival probability due to the electromagnetic dissociation. A comparison with the

data from CMS was performed in bins of the transverse momentum and rapidity. Very good agreement between theory and experiment was found, within the uncertainties.

A.M.S. is supported by the U.S. Department of Energy grant No. DE-SC-0002145 and within the framework of the Saturated Glue (SURGE) Topical Theory Collaboration.

REFERENCES

[1] C.A. Bertulani, G. Baur, «Electromagnetic processes in relativistic heavy ion collisions», *Phys. Rep.* **163**, 299 (1988).

[2] A.J. Baltz, «The physics of ultraperipheral collisions at the LHC», *Phys. Rep.* **458**, 1 (2008).

[3] E. Fermi, «Über die Theorie des Stoßes zwischen Atomen und elektrisch geladenen Teilchen», *Z. Phys.* **29**, 315 (1924).

[4] E. Fermi, «On the theory of collisions between atoms and electrically charged particles», *Nuovo Cimento* **2**, 143 (1925).

[5] C.F. von Weizsäcker, «Ausstrahlung bei Stößen sehr schneller Elektronen», *Z. Phys.* **88**, 612 (1934).

[6] E.J. Williams, «Nature of the High Energy Particles of Penetrating Radiation and Status of Ionization and Radiation Formulae», *Phys. Rev.* **45**, 729 (1934).

[7] M. Cacciari, G.M. Innocenti, A.M. Staśto, «Inclusive open charm photoproduction in ultraperipheral collisions at the LHC with in the generalized photon–nucleus fixed-order next-to-leading logarithm framework», *Phys. Rev. D* **112**, 094029 (2025).

[8] J. Nystrand, «Electromagnetic interactions in nucleus–nucleus and proton–proton collisions», *Nucl. Phys. A* **752**, 470 (2005).

[9] V. Guzey, M. Klasen, «Inclusive dijet photoproduction in ultraperipheral heavy ion collisions at the CERN Large Hadron Collider in next-to-leading order QCD», *Phys. Rev. C* **99**, 065202 (2019).

[10] K.J. Eskola *et al.*, «Spatial resolution of dijet photoproduction in near-encounter ultraperipheral nuclear collisions», *Phys. Rev. C* **110**, 054906 (2024).

[11] S. Frixione, M.L. Mangano, P. Nason, G. Ridolfi, «Improving the Weizsäcker–Williams approximation in electron–proton collisions», *Phys. Lett. B* **319**, 339 (1993).

[12] DELPHI Collaboration (J. Abdallah *et al.*), «Study of tau-pair production in photon–photon collisions at LEP and limits on the anomalous electromagnetic moments of the tau lepton», *Eur. Phys. J. C* **35**, 159 (2004).

[13] ATLAS Collaboration (G. Aad *et al.*), «Observation of the $\gamma\gamma \to \tau\tau$ Process in Pb+Pb Collisions and Constraints on the τ-Lepton Anomalous Magnetic Moment with the ATLAS Detector», *Phys. Rev. Lett.* **131**, 151802 (2023).

[14] (A. Hayrapetyan *et al.*), «Observation of $\gamma\gamma \to \tau\tau$ in proton–proton collisions and limits on the anomalous electromagnetic moments of the τ lepton», *Rep. Prog. Phys.* **87**, 107801 (2024).

[15] CMS Collaboration, «Measurement of the tau g-2 factor in ultraperipheral PbPb collisions recorded by the CMS experiment», CMS-PAS-HIN-24-011, 2024.

[16] D. d'Enterria *et al.*, «Opportunities for new physics searches with heavy ions at colliders», *J. Phys. G: Nucl. Part. Phys.* **50**, 050501 (2023).

[17] ZEUS Collaboration (S. Chekanov *et al.*), «Exclusive photoproduction of J/ψ mesons at HERA», *Eur. Phys. J. C* **24**, 345 (2002).

[18] ZEUS Collaboration (S. Chekanov *et al.*), «Exclusive electroproduction of ϕ mesons at HERA», *Nucl. Phys. B* **718**, 3 (2005).

[19] H1 Collaboration (A. Aktas *et al.*), «Elastic J/ψ production at HERA», *Eur. Phys. J. C* **46**, 585 (2006).

[20] H1 Collaboration (F.D. Aaron *et al.*), «Diffractive electroproduction of ρ and ϕ mesons at HERA», *J. High Energy Phys.* **2010**, 32 (2010).

[21] M.G. Ryskin, «Diffractive J/ψ electroproduction in LLA QCD», *Z. Phys. C* **57**, 89 (1993).

[22] S.P. Jones, A.D. Martin, M.G. Ryskin, T. Teubner, «Probes of the small x gluon via exclusive J/ψ and Y production at HERA and the LHC», *J. High Energy Phys.* **2013**, 085 (2013).

[23] A. Levy, «Exclusive vector meson electroproduction at HERA», in: «Proc. of 12$^{\text{th}}$ International Conference on Elastic and Diffractive Scattering: Forward Physics and QCD», Hamburg May 21–25, 2007, pp. 2–9.

[24] ALICE Collaboration (B. Abelev *et al.*), «Exclusive J/ψ Photoproduction off Protons in Ultraperipheral p–Pb Collisions at $\sqrt{s_{NN}} = 5.02$ TeV», *Phys. Rev. Lett.* **113**, 232504 (2014).

[25] ALICE Collaboration (S. Acharya *et al.*), «Energy dependence of coherent photonuclear production of J/ψ mesons in ultra-peripheral Pb–Pb collisions at $\sqrt{s_{NN}} = 5.02$ TeV», *J. High Energy Phys.* **2023**, 119 (2023).

[26] CMS Collaboration (V. Khachatryan *et al.*), «Coherent J/ψ photoproduction in ultra-peripheral PbPb collisions at $\sqrt{s_{NN}} = 2.76$ TeV with the CMS experiment», *Phys. Lett. B* **772**, 489 (2017).

[27] CMS Collaboration (A. Tumasyan *et al.*), «Probing Small Bjorken-x Nuclear Gluonic Structure via Coherent J/ψ Photoproduction in Ultraperipheral Pb–Pb Collisions at $\sqrt{s_{NN}} = 5.02$ TeV», *Phys. Rev. Lett.* **131**, 262301 (2023).

[28] LHCb Collaboration (R. Aaij *et al.*), «Study of exclusive photoproduction of charmonium in ultra-peripheral lead–lead collisions», *J. High Energy Phys.* **2023**, 146 (2023).

[29] V.P. Goncalves, M.V.T. Machado, «Vector Meson Production in Coherent Hadronic Interactions: An update on predictions for RHIC and LHC», *Phys. Rev. C* **84**, 011902 (2011).

[30] V. Guzey, E. Kryshen, M. Zhalov, «Coherent photoproduction of vector mesons in ultraperipheral heavy ion collisions: Update for run 2 at the CERN Large Hadron Collider», *Phys. Rev. C* **93**, 055206 (2016).

[31] K.J. Eskola *et al.*, «Exclusive J/ψ photoproduction in ultraperipheral Pb+Pb collisions at the CERN Large Hadron Collider calculated at next-to-leading order perturbative QCD», *Phys. Rev. C* **106**, 035202 (2022).

[32] J. Cepila, J. Guillermo Contreras, M. Krelina, «Coherent and incoherent J/ψ photonuclear production in an energy-dependent hot-spot model», *Phys. Rev. C* **97**, 024901 (2018).

[33] B.Z. Kopeliovich, M. Krelina, J. Nemchik, I.K. Potashnikova, «Ultraperipheral nuclear collisions as a source of heavy quarkonia», *Phys. Rev. D* **107**, 054005 (2023).

[34] H. Mäntysaari, B. Schenke, «Probing subnucleon scale fluctuations in ultraperipheral heavy ion collisions», *Phys. Lett. B* **772**, 832 (2017).

[35] A. Adeluyi, C.A. Bertulani, M.J. Murray, «Nuclear effects in photoproduction of heavy quarks and vector mesons in ultraperipheral PbPb and pPb collisions at the LHC», *Phys. Rev. C* **86**, 047901 (2012).

[36] ALICE Collaboration (S. Acharya *et al.*), «Coherent J/ψ and ψ' photoproduction at midrapidity in ultra-peripheral Pb–Pb collisions at $\sqrt{s_{NN}} = 5.02$ TeV», *Eur. Phys. J. C* **81**, 712 (2021).

[37] H1 Collaboration (C. Adloff *et al.*), «Measurement of D^* meson cross-sections at HERA and determination of the gluon density in the proton using NLO QCD», *Nucl. Phys. B* **545**, 21 (1999).

[38] H1 Collaboration (F.D. Aaron *et al.*), «Measurement of inclusive and dijet D^* meson cross sections in photoproduction at HERA», *Eur. Phys. J. C* **72**, 1995 (2012).

[39] ZEUS Collaboration (J. Breitweg *et al.*), «Measurement of inclusive $D^{*\pm}$ and associated dijet cross-sections in photoproduction at HERA», *Eur. Phys. J. C* **6**, 67 (1999).

[40] NNPDF Collaboration (R. Abdul Khalek, J.J. Ethier, J. Rojo), «Nuclear parton distributions from lepton–nucleus scattering and the impact of an electron–ion collider», *Eur. Phys. J. C* **79**, 471 (2019).

[41] M. Cacciari, M. Greco, P. Nason, «The p_{T} spectrum in heavy-flavour hadroproduction», *J. High Energy Phys.* **1998**, 007 (1998).

[42] M. Cacciari, S. Frixione, P. Nason, «The p_{T} spectrum in heavy-flavour photoproduction», *J. High Energy Phys.* **2001**, 006 (2001).

[43] S. Frixione, P. Nason, «Phenomenological study of charm photoproduction at HERA», *J. High Energy Phys.* **2002**, 053 (2002).

[44] R.K. Ellis, P. Nason, «QCD radiative corrections to the photoproduction of heavy quarks», *Nucl. Phys. B* **312**, 551 (1989).

[45] J. Smith, W.L. van Neerven, «QCD corrections to heavy flavor photoproduction and electroproduction», *Nucl. Phys. B* **374**, 36 (1992).

[46] K.J. Eskola, P. Paakkinen, H. Paukkunen, C.A. Salgado, «EPPS21: a global QCD analysis of nuclear PDFs», *Eur. Phys. J. C* **82**, 413 (2022).

[47] R. Abdul Khalek *et al.*, «nNNPDF3.0: evidence for a modified partonic structure in heavy nuclei», *Eur. Phys. J. C* **82**, 507 (2022).

[48] T.-J. Hou *et al.*, «New CTEQ global analysis of quantum chromodynamics with high-precision data from the LHC», *Phys. Rev. D* **103**, 014013 (2021).

[49] P. Aurenche, J.P. Guillet, M. Fontannaz, «Parton distributions in the photon», *Z. Phys. C* **64**, 621 (1994).

[50] E. Reya M. Glück, A. Vogt, «Photonic parton distributions», *Phys. Rev. D* **46**, 1973 (1992).

[51] C. Peterson, D. Schlatter, I. Schmitt, P.M. Zerwas, «Scaling violations in inclusive e^+e^- annihilation spectra», *Phys. Rev. D* **27**, 105 (1983).

[52] E. Braaten, K. Cheung, S. Fleming, T.Ch. Yuan, «Perturbative QCD fragmentation functions as a model for heavy-quark fragmentation», *Phys. Rev. D* **51**, 4819 (1995).

[53] CMS Collaboration (V. Chekhovsky *et al.*), «Measurement of D^0 meson photoproduction in ultraperipheral heavy ion collisions», CMS-HIN-24-003, CERN-EP-2025-095, 2025.

[54] M. Cacciari, P. Nason, «Charm cross sections for the Tevatron Run II», *J. High Energy Phys.* **2003**, 006 (2003).